AIAA JOURNAL
Vol. 45, No. 4, April 2007

Flowfield and Noise Characteristics of Twin Supersonic Impinging Jets

Isaac M. Choutapalli,* Anjaneyulu Krothapalli,† Mehmet B. Alkislar,‡ and Luiz M. Lourenco§
Florida A&M University and Florida State University, Tallahassee, Florida 32310

DOI: 10.2514/1.19914

A way of controlling the acoustic and aerodynamic characteristics of ideally expanded impinging twin jets has been proposed. As a means of control, microjets were used at the nozzle exit. The effect of the controlling method on the flowfield and acoustic field was investigated. Particle image velocimetry was used as the main tool for flowfield diagnostics. The results show that the predominant unsteady character of the impinging twin jets was reduced considerably by the control. Consequently at certain ground plane heights, up to 5 dB reductions in overall sound pressure level of jet noise was observed and up to 25% of the lift loss was recovered. The lift loss recovery was obtained by decreasing the entrainment of the ambient fluid into the main jet and thus lowering suction pressures on the lift plate. On the other hand, no significant effect of control on the fountain flow, which helps lift recovery with upwash, was found.

I. Introduction

WE DISCUSS in this paper the flowfield and noise characteristics of twin impinging jets. The main focus of this work is to examine the role of the fountain flow, generated between the two closely spaced supersonic impinging jets (Fig. 1), on the lift loss and the near-field noise. The simple configuration used in this investigation is similar to that of Krothapalli et al. [1], and the total thrust generated by the two nozzles is nearly identical to that of a single nozzle used in the earlier study. The problem we address here is motivated by the use of twinjets in vertical/short takeoff and landing (V/STOL) aircraft configurations similar to that of the joint strike fighter (JSF). In the course of studying the jet flows in ground effect for the Boeing version of JSF, using twin heated supersonic elliptic impinging jets, strong evidence of the unsteady flow behavior quite similar to that described in this paper was observed.[¶] Hence, it was of practical interest to devise a technique to mitigate the unsteady jet behavior, which is largely responsible for sonic fatigue on the lifting body. A novel control technique using microjet injection at the nozzle exit that was proven to be quite effective in large-scale eddy suppression in single supersonic impinging jet is used in this study [2].

When the wall jets from two jets of equal size and thrust meet, a fountain flow is formed between the jets as shown in Fig. 1. The impingement of the fountain flow on the lift plate produces lift that partially offsets the suckdown force [3]. The suckdown force, commonly referred to as "lift loss," is due to the entrainment flow associated with impinging jets which induce low pressures on the lifting plate, resulting in a force opposite to lift. When twinjets are used, a fountain is created by the interaction of the two impinging jet flows. Such a fountain can produce positive pressures on the underside of the aircraft between the nozzles, thus reducing the lift loss. However, there are conditions under which an increase in the suckdown force as compared to the corresponding single jet is observed (Lummus and Smith [4]). The cause of this additional suckdown appears to be related to the formation of recirculating regions between the fountain flow and each of the adjacent jets. The impingement of the fountain flow on the lift plate produces high pressures in the center region of the plate between the jets, whereas the recirculating flows between the fountain and the jets induce strong suction pressures. Hence, it is of interest to determine the lift loss recovery generated by the twin impinging jets as compared to that of an equivalent single jet. Lummus and Smith also investigated the effect of jet turbulence levels on lift loss. A grid of wires was placed just upstream of the nozzle exit to manipulate the jet turbulence level. It was found that the suckdown increases with increasing levels of turbulence, an aspect that will be addressed later in the paper. Kuhn [3], in a review article, admirably describes the global features of twin impinging jets as they relate to short takeoff and vertical landing (STOVL) aircraft aerodynamics.

Many past basic investigations of twin axisymmetric jet impingement dealt with incompressible jets. Saripalli [5] gives a summary of the results of laser Doppler velocimetry (LDV) measurements obtained in a water channel. One of the key findings of the study was the highly turbulent nature (50% turbulence intensity) of the fountain flow. Flow visualization pictures of high-speed twin impinging rectangular jets suggest [6] that there is a vigorous large-scale collective motion that results in a highly unsteady fountain flow. Preliminary investigations by Elavarasan et al. [7] carried out on a configuration similar to that used in the present study showed that the unsteady coupled motion of the impinging jets dominates the flowfield as shown in Fig. 2. Additionally, they have shown that the fountain flow has an effect on the lift loss and the near-field acoustics. Encouraged by our success in mitigating the large-scale eddies in jets [2,8] and supersonic shear layers [9] with microjet control, we investigate here the role of this control method on the aeroacoustics of impinging twinjet flow.

The main parameters of the problem are the jet exit Mach number, the spacing between the two nozzles, and the impinging plate height. In the present investigation, the jets exit from two identical $M_j = 1.5$ converging–diverging nozzles. From the flow visualization pictures and our past experience in a variety of jet flows, it is expected that the exit velocity profiles are top hat with laminar boundary layers. Although, the spacing between the jets plays an important role in the nature of the jet coupling, in this experiment it is fixed at three diameters. The height of the impinging plate with respect to the nozzle exit is varied from 2 to 20 nozzle diameters.

Presented as Paper 3316 at the 9th AIAA/CEAS Aeroacoustics Conference, Hilton Head, SC, 12–14 May 2003; received 6 September 2005; revision received 12 May 2006; accepted for publication 19 May 2006.

*Graduate Research Assistant, Department of Mechanical Engineering, 2525 Pottsdamer Street; cisaac@eng.fsu.edu. Member AIAA.
†Don Fuqua Eminent Scholar, Department of Mechanical Engineering, 2525 Pottsdamer Street. Associate Fellow AIAA.
‡Research Scientist, The Boeing Company, Seattle, WA. Member AIAA.
§Professor, Department of Mechanical Engineering, 2525 Pottsdamer Street. Member AIAA.

¶Private communication with A. Krothapalli, 2001.

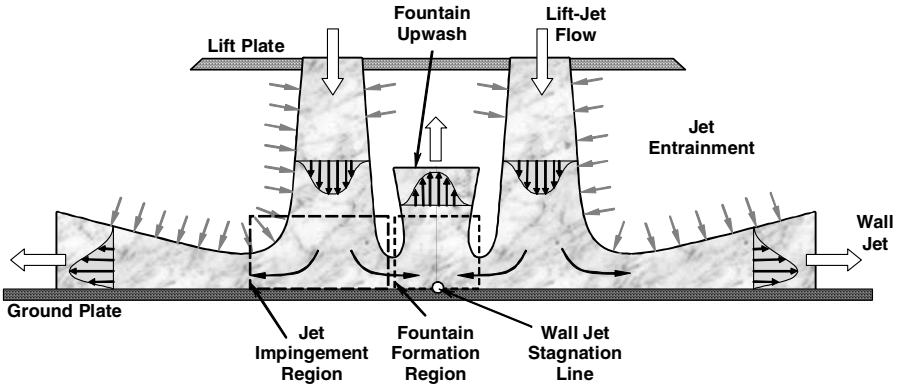

Fig. 1 Schematic of the twinjet impingement flowfield.

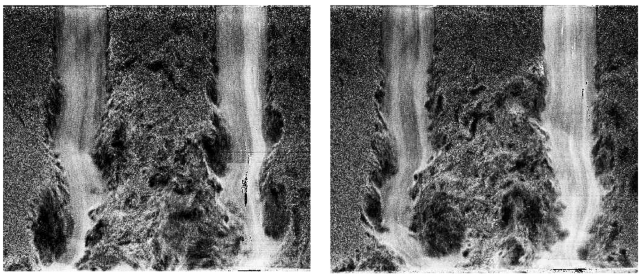

Fig. 2 Instantaneous flow visualization pictures of the twinjet flowfield [7]. $M = 1.5$, $h/d_s = 4$ (h = height of the impinging plate with respect to the nozzle exit, d_s = equivalent single nozzle diameter).

II. Experimental Apparatus and Procedures

The experiments were conducted in STOVL supersonic jet facility of the Fluid Mechanics Research Laboratory located at the Florida State University (Fig. 3). The facility was designed to obtain the jet-induced forces on a STOVL aircraft model hovering in and out of ground effect. To simulate the hover effect, the distance between the ground plane and the jet nozzle exit was varied by moving the ground plane up and down relative to the nozzle exit through a remote-control hydraulic lift incorporated with the facility. For the experiments described here, the ground plane was 2.44×2.44 m and was centered underneath the model. To have an instrumented ground plane for ground erosion studies, a 25.4 mm thick aluminum plate having dimensions of 0.7×0.7 m was mounted on top of the larger ground plane. The hydraulic lift allowed the height between the ground and nozzle exit (h) to vary from 0.04 to 1.5 m.

The measurements are carried out with shock-free, nearly ideally expanded jets. The two identical nozzles are mounted on a plenum chamber assembly as illustrated in Fig. 4. Each jet exits from a converging–diverging (C–D) axisymmetric nozzle with a throat diameter of 18 mm designed for an exit Mach number of 1.5. The exit diameter d of the C–D nozzle is 19.5 mm. The divergent section is intentionally made of straight conic section with a 3 deg divergence angle to mimic the realistic nozzle geometry used in practice. The distance between the nozzle centers is 58.5 mm ($\sim 3d$). The scaling parameters used in the present study are guided by the earlier experiments of Wardwell et al. [10]. The combined exit area of the two nozzles was identical to that of a single nozzle used in Krothapalli et al. [1]. As a result, the fountain flow effects can be easily delineated. An aluminum plate 254 mm in diameter is flush mounted with the nozzles, which served as the lift plate.

The lift plate contains 48 pressure taps arranged along radial and circumferential directions covering one quarter of the lift plate (as indicated in Fig. 4b by dotted lines). The holes were spaced unevenly with closer spacing near the nozzle exit. The pressures were measured with a Validyne strain-gauge transducer mounted in a scanivalve unit. At each port, several seconds of digitized data were taken and processed later to obtain the mean surface pressure. The

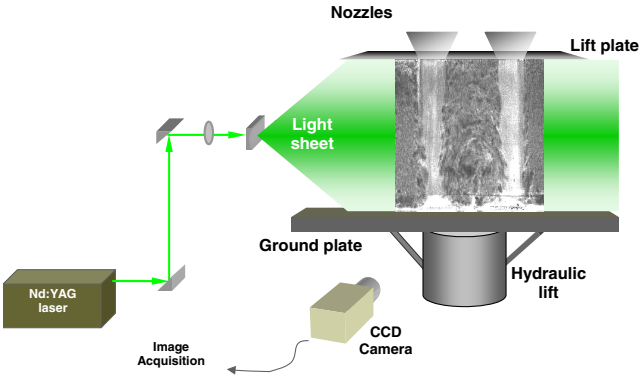

Fig. 3 Schematic arrangement of twin supersonic jet apparatus with the PIV setup.

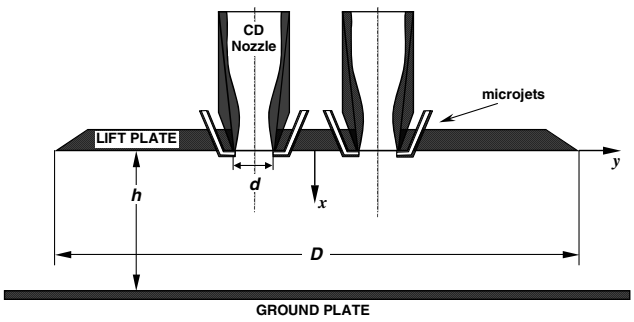

a)

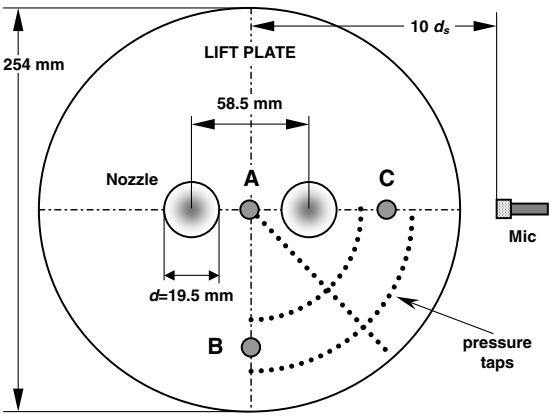

b)

Fig. 4 a) Illustration of the lift plate, twin nozzles, and the ground plate. b) Illustration of lift plate and instrumentation; Kulite transducer locations are indicated by A, B, and C.

jet-induced mean surface pressures on the plate were used to calculate the lift force. The unsteady surface pressure was measured using three Kulite pressure transducers located strategically on the lift plate. The signals are passed though a low-pass filter with a cutoff frequency of 33 kHz before being digitized, with a sampling rate of 70 kHz, by a National Instruments data acquisition card.

A quarter-inch Bruel & Kjaer microphone (type 4136) with preamplifier (type no. 2690A) was used for near-field acoustic measurements of jet noise. This microphone has a flat response up to 70 kHz and can be exposed to noise levels of about 170 dB. The location of the microphone is chosen to be 10 equivalent diameters away from the jets as shown in Fig. 4b. The acoustic data are low-pass filtered with a cutoff frequency of 50 kHz, and acquired with a sampling rate of 110 kHz.

The air supply for the jet was provided from high-pressure (15 MPa) storage tanks coupled to a high displacement air compressor. The tanks are capable of providing a total capacity of 10 m^3 and can drive the twin Mach 1.5 jets continuously up to 40 min. The main controlling parameter in the experiment is the ground plate height h with respect to the nozzle exit, which was varied from $2d_s$ to $5d_s$, where $d_s(=27.5$ mm) corresponds to an equivalent single jet exit diameter. The experiments were conducted at a nozzle pressure ratio (NPR) of 3.7 (stagnation pressure/ambient pressure), which is the ideally expanded jet condition of the nozzle. The jet stagnation temperature was maintained at 293 ± 2 K. The nominal exit Reynolds number, based on the exit velocity U_j and nozzle diameter d, was about 5.5×10^5. The coordinates x and y correspond to axial and radial directions of the jet, and u and v are respective velocity components. The origin of the coordinate system is centered on the lift plate (Fig. 4a).

The microjet actuation is done by using 16 microjets generated from a high-pressure bottled nitrogen source and exiting from 400-μm-diam tubes. The microjets then enter the primary jet at an angle of 90 deg to the nozzle axis (Fig. 4a). The microjet-based control procedure is an open-loop scheme, that is, there is no feedback. Nitrogen from a high-pressure gas cylinder was led to a cylindrical manifold through a pressure regulator, from which it was distributed to the 400 μm stainless steel tubes for creating the microjets. A precision mass flow meter was used to monitor the combined microjet discharge. In the present experiments, a combined mass flow rate of 0.0025 kg/s was used; this value corresponds to about 0.6% of the primary jet mass flux. The aforementioned microjet mass flow rate was possible by maintaining effective stagnation conditions of $P_{0mj} = 100$ psig and $T_{0mj} = 300$ K. With these conditions, the microjet tube exit flow was choked and the fully expanded Mach number was supersonic, having a value of about 2.

For planar particle image velocimetry (PIV) measurements, a double-pulsed, digitally sequenced Nd:YAG laser (Spectra Physics PIV400) was used. A light sheet of approximately 1 mm thickness was created by suitable combination of spherical and cylindrical lenses (Fig. 3). A cross-correlation CCD camera (Kodak ES1.0) with a resolution of 1008(H) $\times$ 1018(V) pixels of a size of 9×9 μm^2 was used for recording the images. The camera was fitted with a 50 mm (f/2.8) Nikon lens. The image area covered was 215×228 mm. In the present experiment, 15 image pairs per second were acquired with time between two successive images in a pair being 2.5 μs for the jet flow and 18 μs for the entrained flow measurements. The camera was positioned at 90 deg to the jet axis (Fig. 3). The jet was seeded with submicron ($\sim$0.3 μm) oil droplets generated by a modified Wright nebulizer. The flow rate of the seeding particles was controlled in such a way that there were enough particles in the jet. The ambient air was seeded with smoke particles (1–5 μm) produced by a Rosco fog generator. The velocity data with high spatial resolution are achieved with the novel processing algorithm developed by Lourenco and Krothapalli [11]. A summary of the procedure used in this algorithm is given in a recent paper by Alkislar et al. [12]. The salient feature of this adaptive integration window approach is that the flowfield at any point in the image is described with second-order accuracy including the derivatives. Even though an unstructured grid is used for obtaining the velocity vectors, the velocity field in the present study is presented at regular interval for ease of presentation. Mean and turbulent velocity fields were computed by processing 1000 image pairs, thus giving an accuracy of better than 1 and 5% in mean velocity and turbulence intensity measurements, respectively. For a more detailed discussion of the PIV setup, reference can be made to Alkislar et al.

III. Results and Discussion

A. Flow Visualization

A conventional shadowgraph technique was used to visualize the twin impinging jet flow. The images were captured using an SVHS video camera. Images displaying important flow features are shown in Fig. 5 at two different time instants representative of two different phases of the resonance condition for $h/d_s = 4$ and $h/d_s = 2$. The resonance condition is brought about by the feedback loop, the mechanism of which is discussed at length in Krothapalli et al. [1]. The energy for the feedback loop is provided by the instability waves in the shear layers of the jet. These waves are generated by acoustic excitation in the region near the nozzle exit. The waves grow as they propagate downstream and manifest themselves as large-scale vortical structures. Upon impingement on the ground plane, these large structures generate coherent pressure fluctuations, which result in acoustic waves with significant intensity. These acoustic waves travel through the ambient medium and upon reaching the nozzle exit, excite the shear layer of the jet, leading to the generation of instability waves, thus closing the feedback loop.

The shadowgraph images show that the dominant feature of the jet flow is the flapping motion of the individual jets. In addition, both the jets appear to oscillate in synchronous fashion, giving rise to a symmetric mode with respect to the midplane separating the two jets. The two jets, after impinging on the ground plane, spread radially along the wall, forming the wall jets symmetrically around the jet axes. Between the two main jets, a stagnation region created by the collision of the wall jets gives rise to a fountainlike flow. At lower h/d_s, the fountain upwash was observed to reach the lift plate between the two nozzles as shown in Fig. 5. At higher $h/d_s(=4, 6)$ shown in Figs. 5 and 6, respectively, the fountain flow does not reach the lower surface of the lift plate. It can be further noticed from the figures that as the distance of the ground plane from the nozzle exit is increased, the vertical extent of the fountain flow decreases. It might be reasonable to say that the fountain flow would disappear if the ground plane is moved to a location that is beyond the point where the twin jets merge to become a single jet.

An examination of the continuous video record of the shadowgraph images suggests that the axisymmetric freejet instability manifests itself in symmetric as well as helical and/or flapping modes. But most often the two jets are dominated by the helical mode instability. The type of instability depends on the exit Mach number, NPR (i.e., over expanded/underexpanded), the characteristics of the exit boundary layer, and the proximity of the ground plane to the nozzle exit (Krothapalli et al. [1]). The mode shape is also largely decided by the characteristics of the instability wave, which is a source of energy for the feedback mechanism (Tam

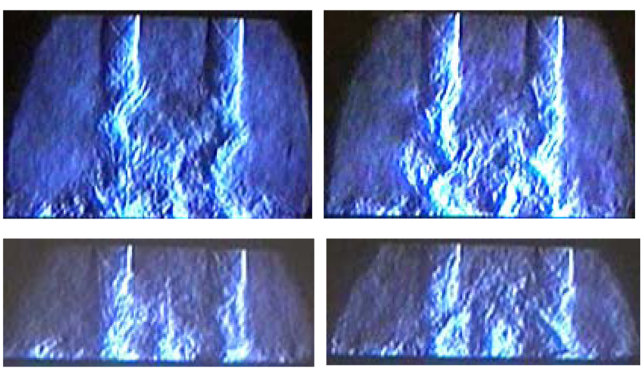

Fig. 5 Shadowgraph pictures of twin impinging jets, $M_j = 1.5$. Top:$h/d_s = 4.0$, bottom:$h/d_s = 2.0$.

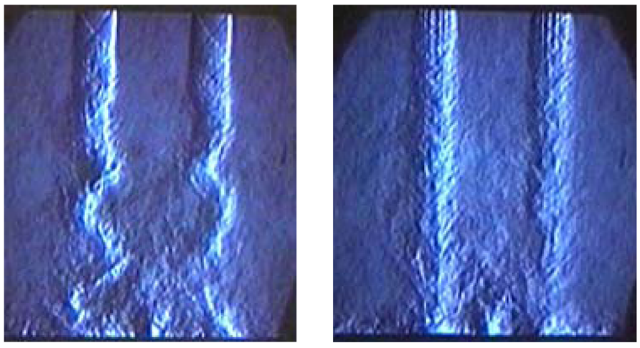

Fig. 6 Shadowgraph pictures of the twin impinging jet at $h/d_s = 6$, $M_j = 1.5$ without (left) and with (right) control.

[13]). The distance of the ground plane with respect to the nozzle exit influences the characteristics of the instability wave to a large extent. The studies of Krothapalli et al. [1] on a single impinging jet have shown that the jet is dominated by a helical mode as the ground plane is moved closer to the nozzle exit. Similar observations are also made in the present study at $h/d_s = 2$ and 4. The individual jets oscillate with counterrotating helical oscillation modes. The coupling between the jets results in a symmetric mode with respect to the midplane separating the two jets. A similar observation was made by Alkislar et al. [14] for corresponding twin freejets and for two underexpanded screeching jets that are spaced closer ($1.9d$) than the current setup by Seiner et al. [15]. The sinuous oscillation of individual jets is a result of self-excitation due to screech. Owing to the straight divergent section, a weak shock cell structure is present in the jet. Together with the presence of lift plate, an intense screech tone is generated. The symmetric coupling mode with the helical mode being dominant in individual jets is vividly shown in Fig. 6. The violent motion of the jets is arrested by the use of microjets as depicted in Fig. 6 for $h/d_s = 6$. The streaks seen at the nozzle exit are due to streamwise vortices that are generated by the interaction of the microjets with main jet. In the following section, we will examine the near-field acoustics and flowfield characteristics with and without control.

B. Unsteady Surface Pressure and Near Sound Field Characteristics

The most violent oscillations of the twin impinging jets are found at $h/d_s = 4$, and the strongest fountain flow is observed at $h/d_s = 2$. Therefore, we will examine the narrowband frequency spectra of the surface pressure signals on the lift plate and the near-field microphone at these conditions as shown in Fig. 7. At $h/d_s = 4$, the spectra depict a strong discrete tone at 5.8 kHz, which is referred to as the impinging tone. At the present jet operating condition, because of the presence of the lift plate and weak shock cell structure, a screech tone ($f = 6.7$ kHz) at substantial reduced amplitude is also observed. The distinction between the screech and impinging tones is made based on examining their variation with h/d_s (cf. Figure 8). The other discrete tones seen in the spectra are either the harmonics or combinations of the two dominant frequencies: screech tone and the impinging tone. The frequency spectrum of the Kulite A signal placed in between the nozzles is quite similar to that of the Kulite C (Fig. 7c) and the corresponding overall sound pressure levels (OASPLs) (165 dB) are also nearly identical (cf. Figure 9). Hence the fountain flow seems to have negligible effect on the unsteady surface pressure for $h/d_s = 4$. However, in the direction normal to the plane containing the jet axes, the tone intensities are lower (Kulite B), resulting in lower OASPL of about 160 dB. When compared to single equivalent impinging jet at the same jet operating conditions, we find generally that the OASPL at the location of Kulite B is much reduced ($\sim$5 dB), whereas negligible effect is found at the Kulite C location by the twinjet arrangement. These observations suggest that the jet

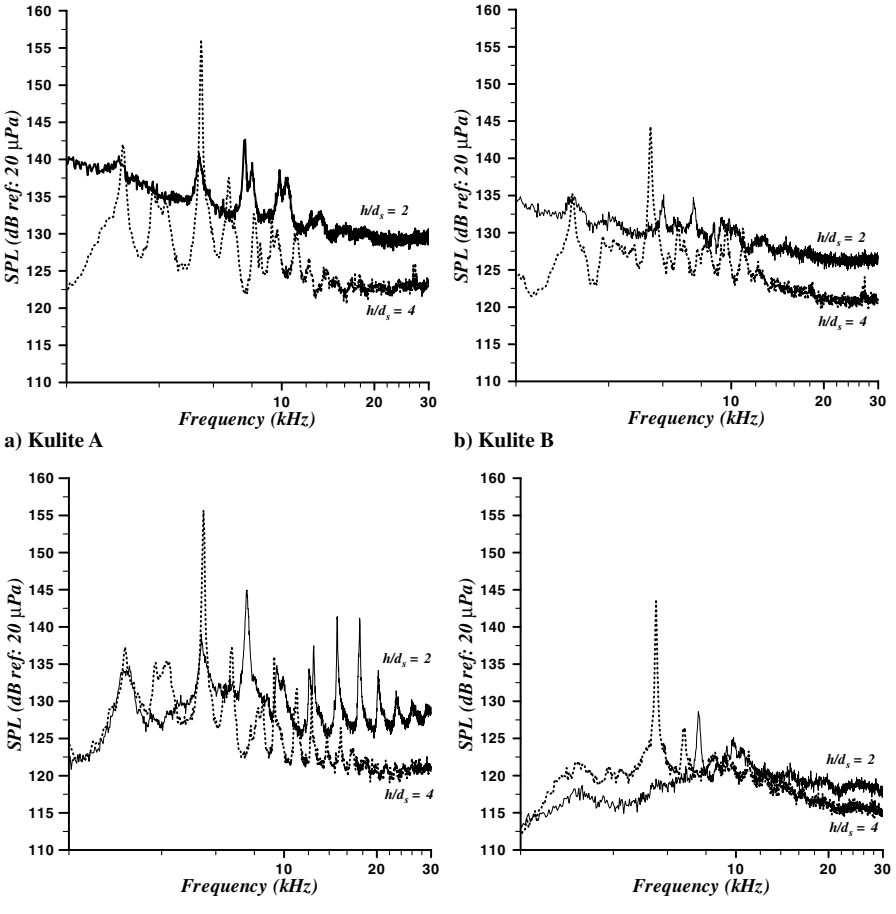

Fig. 7 Spectra, lift plate surface pressure signals, and microphone for $h/d_s = 2$ and $h/d_s = 4$.

coupling is mostly confined to the plane containing the jet axes, which is consistent with the results of instability analysis of twin axisymmetric freejets [16]. The reduction of OASPL in the direction normal to the flapping plane is similar to that observed in elliptic [17] and diamond-shaped jets [18].

When a strong fountain is formed at lower h/d_s, the sound pressure levels (SPLs) of the surface pressure signals are higher than those at $h/d_s = 4$, as shown in Fig. 7. The largest increase of OASPL (5 dB) is found in between the jets, where the fountain flow impinges on the lift plate. The impinging tones are most dominant in the spectrum of the Kulite C signal, which is located in the plane of the flapping motion of the jets.

The near-field microphone signal, however, shows the absence of significant tones. Based on these observations and also from the observations of previous studies (Krothapalli et al. [1], Alvi et al. [2]), it appears that the contributions of the fountain flow to the surface pressure fluctuations are significant only when $h/d_s < 4$.

Because the oscillatory behavior of jets is quite similar to that of a single equivalent jet, it is believed that the phenomenon associated with discrete sound generation is governed by a simple feedback loop as discussed in Krothapalli et al. [1]. The impingement tone frequency f_N is determined from the following formula proposed by Powell [19]:

$$\frac{N+p}{f_N} = \int_0^h \frac{\mathrm{d}h}{C_i} + \frac{h}{C_a}; \qquad N = 1, 2, 3 \ldots . \tag{1}$$

Here h is the distance between the wall and the nozzle exit and C_i and C_a are the convection velocities of the downstream traveling large structures and the speed of upstream traveling acoustic waves, respectively.

N is an arbitrary integer and p represents a phase lag due to the fact that the phases of the acoustic wave and of the convected disturbance are not always exactly equal at both the nozzle exit and the source of sound. In using the formula to predict the discrete frequencies, the values for convection velocities and the phase delay p are taken from our earlier single equivalent jet measurements. The solid lines shown in Fig. 8 represent the predicted frequencies using the feedback formula [Eq. (1)]. The measured frequencies are in good agreement with those of the prediction formula. It can be seen from the figure that the measured frequencies fall in close proximity to one of the predicted frequencies. To see which one of the measured frequencies agrees more closely with the predicted frequencies, a substantial number of predicted frequencies have been plotted by changing the value of n in Eq. (1). Hence it can be said from the observations made in Fig. 8 that the self-sustained jet oscillations are caused by the same mechanism as that observed in the single impinging jet [1]. The data plotted in the fashion (Fig. 8) show clearly the screech tone that is identified with respect to twin freejets [14], which is designated in the figure as f_{freejet}. For $h/d_s > 10$, only screech tone and its harmonics

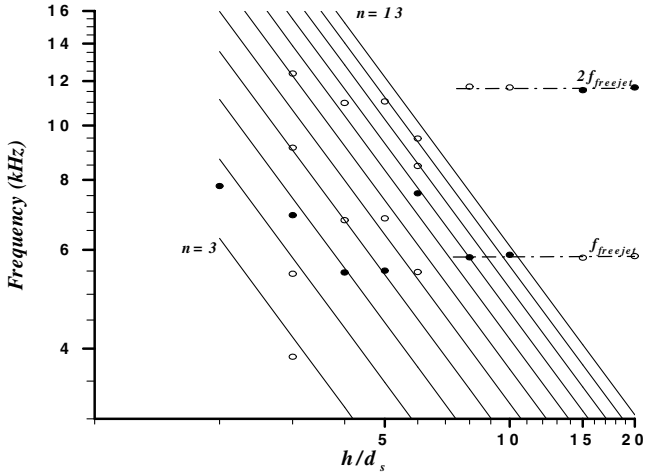

Fig. 8 Impinging tone variation with ground plane distance. Filled symbols represent amplitude dominant tones.

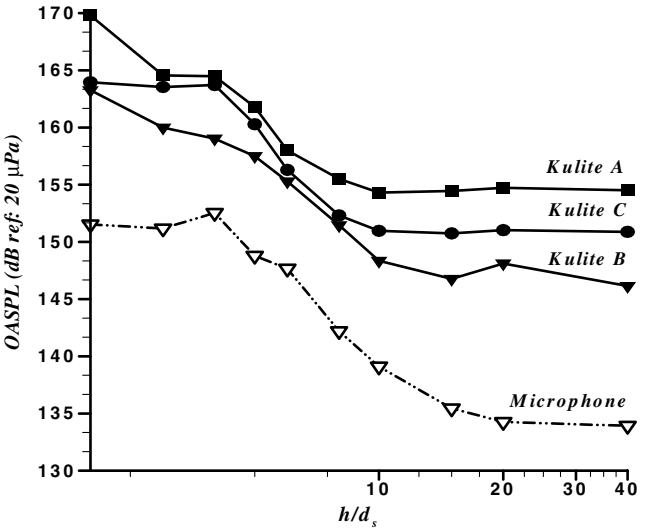

Fig. 9 Overall sound pressure level variation with ground plane distance.

are observed. The mechanism for the screech tone generation is a feedback loop that is well understood. The presence of a second jet in the immediate neighborhood will slightly alter screech characteristics in a manner that the resulting twinjet Strouhal number is less than its corresponding single equivalent jet.

In addition to the discrete tones generated due to a feedback loop as described earlier, the broadband components of the spectrum also change with impingement. From the near-field narrowband spectra, such as those shown in Fig. 7, overall sound pressure levels were calculated and plotted as a function of h/d_s in Fig. 9. The data obtained using surface-mounted Kulite transducers and near-field microphone are included in the plot. To show the rapid changes in close proximity of the ground plane, the data are plotted in a semilogarithmic form. The sound pressure level decreases with increasing h/d_s, reaching close to its freejet value at about $h/d_s = 20$. The increase in OASPL due to impingement is about 15 dB at $h/d_s < 5$ as compared to about 8 dB for an equivalent single jet [1]. The OASPLs of the Kulite pressure transducer's signals on the lift plate and the near-field sound are generally lower than those produced by a corresponding single equivalent jet, except when the fountain flow impingement is dominant at lower values of h/d_s. For example, Fig. 10 shows the near sound field OASPL variation with ground plane distance for twinjets and the corresponding single equivalent jet to confirm the finding discussed earlier in this section. Note that the microphone is located in the plane of the twinjets (Fig. 4b).

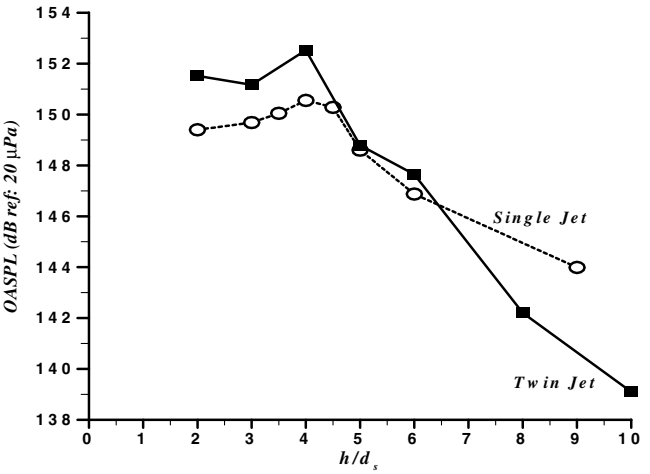

Fig. 10 Near-field microphone OASPL variation with ground plane distance for twinjets and equivalent single jet.

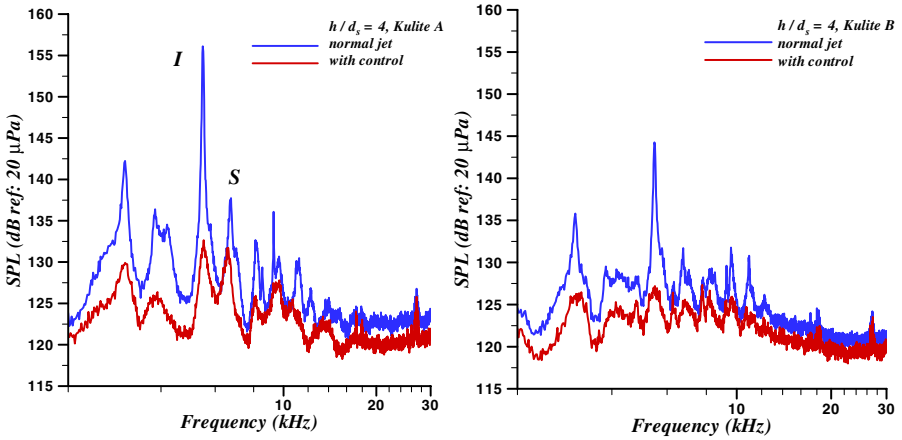

Fig. 11 Effect of microjet injection on the surface pressure frequency spectra.

The OASPL reductions seen for $h/d_s > 6$ are due to shielding effect (outboard jet serves to "shield" some of the noise of the inboard jet from a sideline observer) commonly observed in multiple jet arrangement [20].

C. Effect of Microjet Control

The effect of the microjet injection on the unsteady surface pressure and the near-field sound are discussed in this section. The data included here correspond to $h/d_s = 4$ where the flow visualization pictures show the most vigorous oscillations. The narrowband frequency spectra of the Kulites A and B signals shown in Fig. 11 clearly indicate that, with the activation of the microjets, the impingement tone is suppressed along with noticeable reduction in the broadband noise. The impinging and screech tones are identified in the figure by letters *I* and *S*, respectively. Broadband reduction in noise levels indicates an overall decline of the unsteadiness in the flow under control as confirmed by the flow visualization pictures. At this condition, the microjet injection reduces the OASPL by about 5 dB, whereas modest reductions of about 2 dB are observed at other heights. The reduction is thought to be associated with the disruption of the feedback loop that creates the discrete impinging tones, leading to a marked reduction in the unsteadiness of the flow. Apart from the reduction in the OASPL, it can also be seen from Fig. 11 that there appears to be frequency shift in the screech tone when microjet control is applied. The frequency shift in the spectrum is due to changes in the shock cell structure when the microjets are activated. The variation of the centerline velocity (cf. Fig. 18) indicates a modified shock cell structure. It is well known that the screech phenomenon is generated by disturbances in the shear layer, which convect downstream and come into contact with a shock cell boundary. This interaction, particularly at the end of a shock cell, results in the generation of intense sound. A small change in the shock cell structure with the application of microjets could perhaps be the reason for the frequency shift in the spectrum.

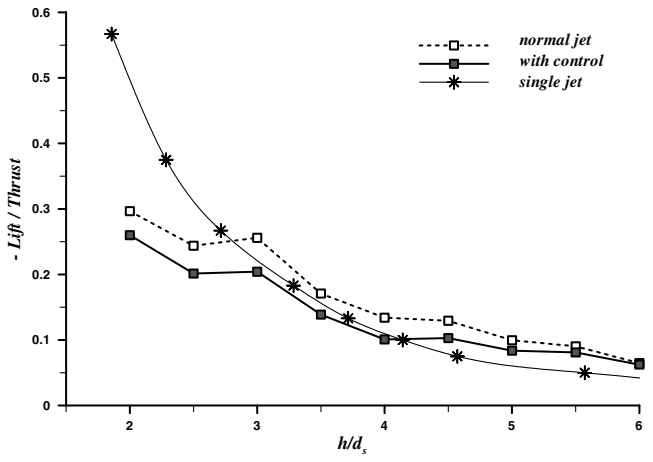

Fig. 12 Lift loss variation with impinging plate height.

D. Hover Lift Loss

The lift force induced by the jet and fountain flows on the lift plate was obtained from the integration of the mean surface pressure. The force obtained was normalized by the total jet thrust of both jets calculated from one-dimensional isentropic relations. In Fig. 12 the comparison of lift loss due to normal and controlled jets as a function of h/d_s is given. Also included in the figure are the data for a single jet with same equivalent diameter. As the ground plane approaches the lift plate, a large downward force is generated on the lift plate. Single jet data show that at very close distances the lift loss is about 60% of the thrust. However, for twinjet configuration the lift loss is only about 30%; the fountain flow increases the pressure between the nozzles, negating the suction effect caused by the entrainment. As the ground plane distance increases, the fountain flow effect diminishes and the twinjets have a higher lift loss than the corresponding single jet. The reason for this diminished effect is that the fountain flow weakens for distances $1.5d_s$ above the ground plane irrespective of the h/d_s. It appears that the effect of the fountain on thrust loss is confined to about $h/d_s < 2.5$.

At larger ground plane distances close to freejet conditions, the lift loss is larger for twinjet flow compared to single jet. Although the area is equivalent for both jet flows, the periphery of the jets is increased for twinjets by a ratio of 1.4. A larger jet boundary increases the amount of entrainment from the ambient air, which is directly related to the suckdown force on the lift plate. For $x/d_s < 6$, with microjet control, an improvement in the lift loss is observed. The role of microjet control on the elimination of large scale structures in the twinjet flow is clearly shown in the PIV images (Sec. III.E, Fig. 13). It can be seen that the large-scale structures at $h/d_s = 2$ and 4 are eliminated and the unsteady oscillations of the jets are suppressed. The elimination of these structures decreases the entrainment flow over the lift plate and results in modest recovery of the lost lift. Up to 25% lift loss recovery was obtained with control at $h/d_s < 4$. After a distance of $h/d_s = 6$, no significant change is observed within the experimental accuracy. Hence, the maximum lift loss recovery occurs for small heights with the influence becoming less significant for larger heights. These observations clearly suggest that twinjet arrangement helps to reduce the suckdown force as compared to that of equivalent single jet at ground heights where the lift loss is most dominant.

E. PIV Flowfield Measurements

The flow details were captured by means of PIV measurements. The PIV images are also used as flow visualization to observe the global behavior of the jets captured at an instant as shown in Figs. 13 and 14 corresponding to $h/d_s = 2$ and 4, respectively. The unsteady

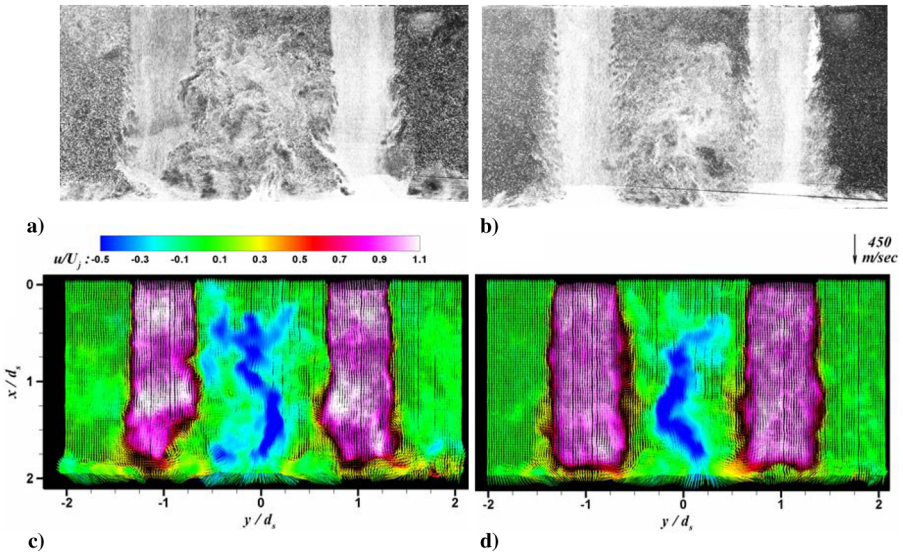

Fig. 13 Instantaneous PIV images at $h/d_s = 2$, a) normal jet, b) with control; corresponding velocity vector-vorticity fields, c) normal jet, d) with control.

behavior of the jet at $h/d_s = 2$ is captured in Fig. 13a. This figure shows the view of the impinging jet at an instant when the main jets are characterized by prominent large-scale structures. These large-scale structures appear symmetrically with respect to the central plane between the two jets. Because the jets are highly unsteady, the location of the stagnation point or the fountain jet origin changes randomly in the region between the main jets and frequently interacts with the main jets. With the use of microjets, the flapping motion of the individual jets is mostly suppressed and relatively steady flow replaces the violent oscillations as captured in Fig. 13b. The fountain jet appears to nearly reach the lift plate. Also seen in the figure are the standoff shocks near the impinging plate, noted by the sharp particle density variations.

The instantaneous uniformly scaled velocity vectors corresponding to images in Figs. 13a and 13b are shown in Figs. 13c and 13d. These velocity fields clearly show the reduction in the violent fluctuations in the flow with the use of control. The normalized axial velocity color contours are shown in the figure. The weak shock cell

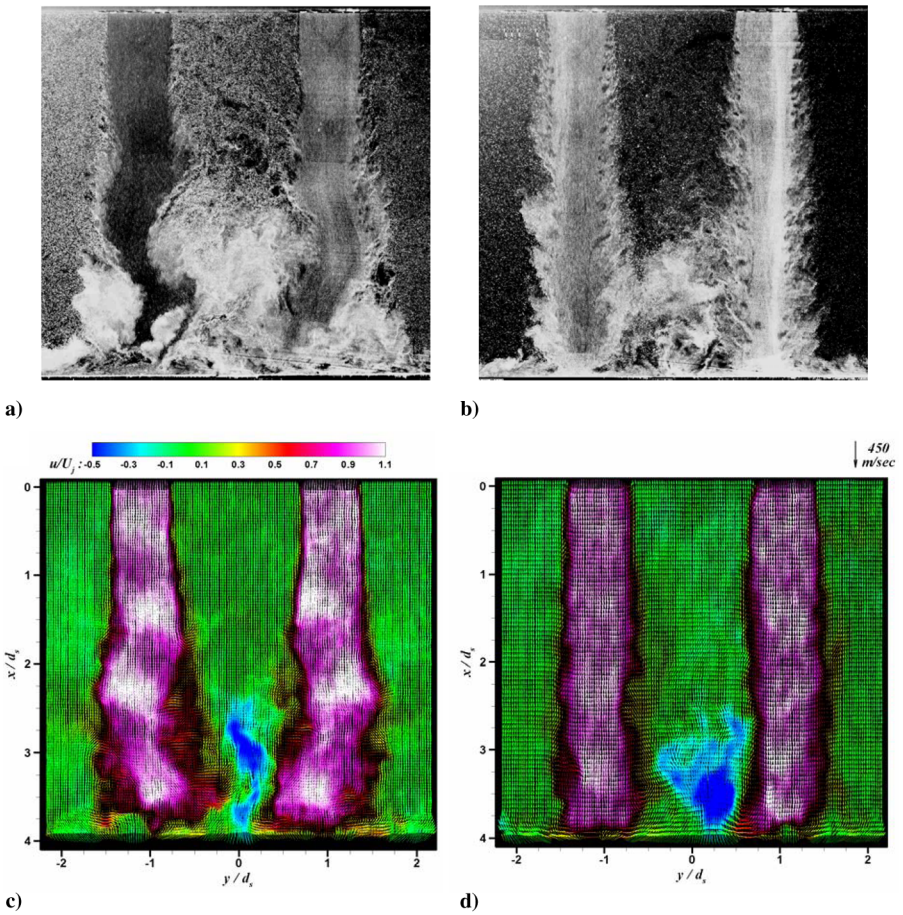

Fig. 14 Instantaneous PIV images at $h/d_s = 4$, a) normal jet, b) with control; corresponding velocity vector-vorticity fields, c) normal jet, d) with control.

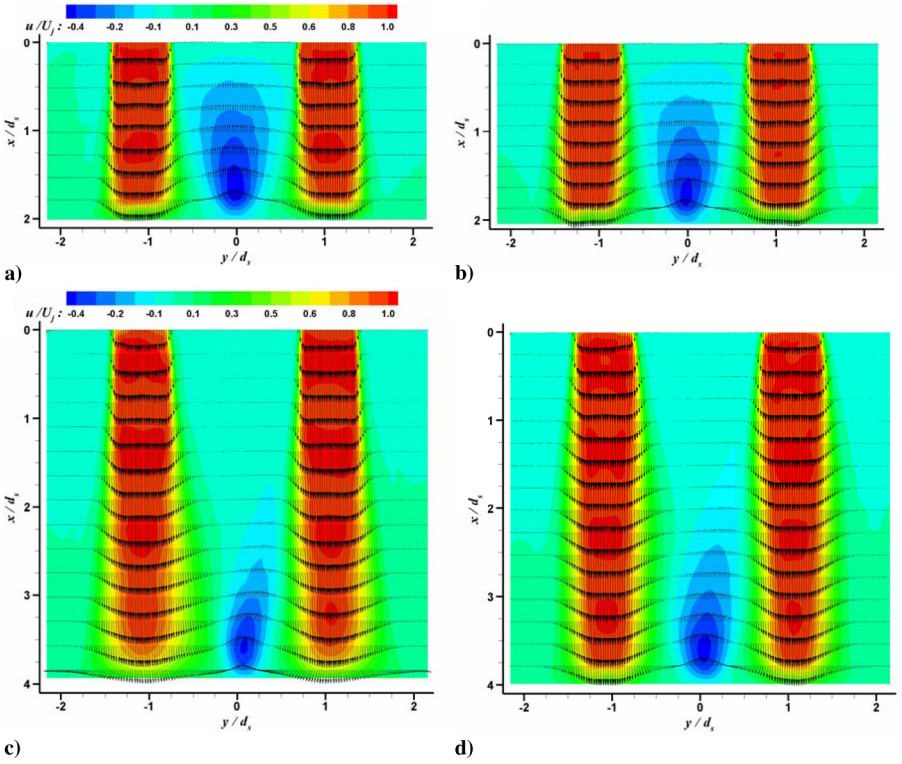

Fig. 15 Mean velocity field; a) normal jet at $h/d_s = 2$, b) with control at $h/d_s = 2$, c) normal jet at $h/d_s = 4$, d) with control at $h/d_s = 4$.

structure is depicted by the presence of the high-velocity regions with contour levels greater than 1.0. The fountain region is marked by the contour levels between −0.25 and −0.5, with a highest velocity of about 200 m/s. The fountain jet almost reaches the lift plate resulting in significant lift loss reduction as observed in Fig. 12. The measurements at $h/d_s = 4$, shown in Fig. 14, suggest that the fountain flow appears to diminish within about $1.5d_s$ from the ground plane suggesting that its effect on lift loss recovery will be quite minimal, in support of the lift plate pressure measurements shown in Fig. 12. Vigorous large-scale oscillations of the individual jet column are quite apparent in the PIV image and in its corresponding vector field. These oscillations are reduced considerably with microjet control.

F. Mean Velocity Field

To investigate the mean flow behavior, 1000 instantaneous velocity fields were averaged. The mean velocity fields in the central plane of the flowfield for two different h/d_s with and without control are shown in Fig. 15.

The normalized u-velocity contours along with a selected number of velocity profiles are shown in the figure. The fountain jet is marked by the contour levels between −0.25 and −0.5. The slight asymmetry seen in the fountain jet at $h/d_s = 4$ is attributed to slight misalignment of the ground plate with respect to the jet axes, which becomes noticeable at larger ground heights. However, many important observations made here will not be affected by this asymmetry in the fountain flow. From the data shown in Fig. 15, it appears that the maximum penetration of the fountain jet is limited to about $1.5d_s$. Because the penetration height is a strong function of the jet velocity and the spacing between the jets, the preceding observation is limited to the conditions of the present experiment. The microjet control seems to have negligible influence on the penetration height of the fountain while reducing significantly its unsteadiness.

The strength of the fountain flow can be characterized by the mean axial velocity variation along the centerline as shown in Fig. 16. The data shown here are extracted from the mean velocity fields of Fig. 15. The maximum velocity magnitude is nearly the same for

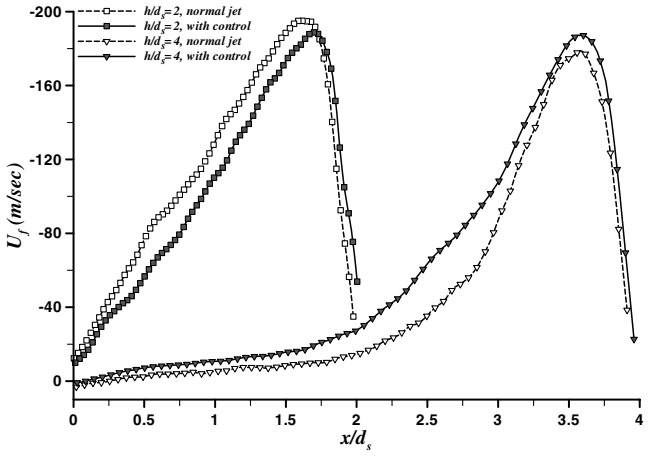

Fig. 16 Fountain flow centerline mean axial velocity profiles at $h/d_s = 2$ and $h/d_s = 4$.

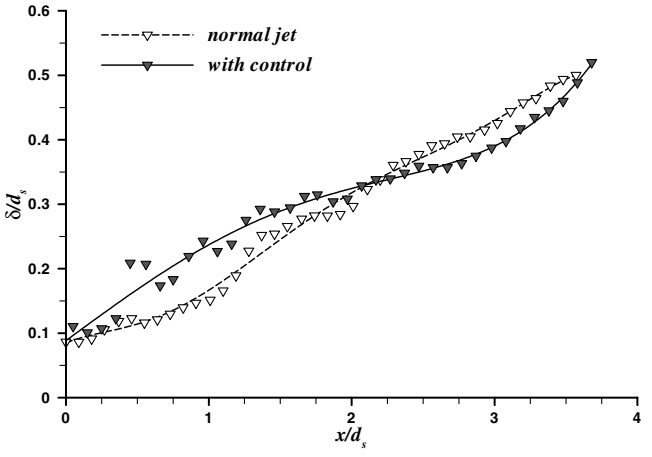

Fig. 17 Comparison of the outer shear layer growth of the jet with and without control for $h/d_s = 4$.

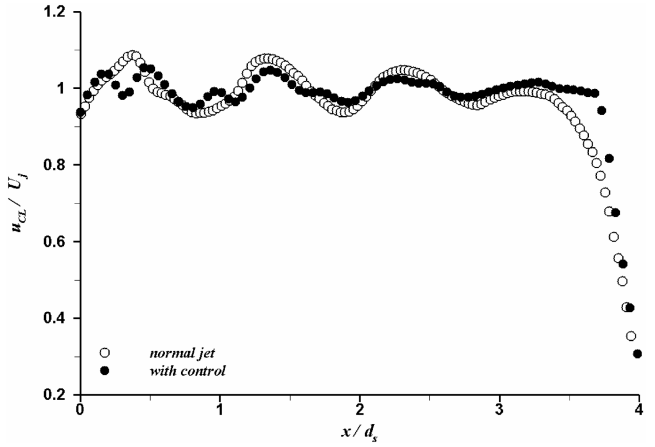

Fig. 18 Comparison of the mean centerline axial velocity of the jet with and without control for $h/d_s = 4$.

both the cases. The location at which the maximum velocity occurs is $0.5d_s$ from the ground plane and it appears to be independent of the ground height. For $h/d_s = 4$, most of the fountain momentum is lost before it reaches the lift plate, thus having an insignificant effect on lift loss recovery. Marginal changes are seen in the fountain with control.

To determine the effect of microjet control, the shear layer growth on the outer side of the jets was calculated using the mean velocity-field data. The shear layer thickness δ was defined as the transverse distance (y coordinate) between the locations where the axial velocity was equal to 5 and 95% of the local axial velocity at the jet centerline. The data obtained for $h/d_s = 4$ are shown in Fig. 17. For the normal jet, it appears that initially, the shear layer grows slowly at the nozzle exit followed by a rapid increase for $x/d_s > 1$ due to the presence of large eddies. With control, the initial shear layer of the jet increases in thickness due to the presence of streamwise vortices that are generated by the interaction of microjets with the shear layer [9,21]. These vortices initially increase the shear layer thickness; however, at the downstream locations they disturb the growth of large-scale eddies via reducing the spatial coherence of the azimuthal structures due to the three-dimensionality of the shear layer. Consequently, a reduced growth rate in the shear layer is observed further downstream of $x/d_s > 2$. Although not shown in the figure, similar behavior was observed for the inner shear layer of the jets. These observations are consistent with those of Arakeri et al. [8].

The effect of microjets is further investigated by examining the centerline velocity decay of jets. The jet centerline mean axial velocity variation with and without control is shown in Fig. 18. The small undulations seen in the data are due to the presence of weak shock cell structure. With activation of microjets, except for a small reduction in undulation amplitude (indication of weakened shock cell structure), the jet centerline velocity variation is marginally affected. An examination of the normalized radial velocity and vorticity profiles at successive downstream locations will indicate the effect of the control method on the global flow characteristics. In Fig. 19, we present the axial mean velocity and out-of-plane vorticity component profiles in a suitably normalized form for $h/d_s = 4$.

Also included in the figure are the corresponding profiles with microjet activation. Here, $R_{1/2}$ is the radius at which $U/U_j = 0.5$. As is customary, the profiles are plotted with their origin being

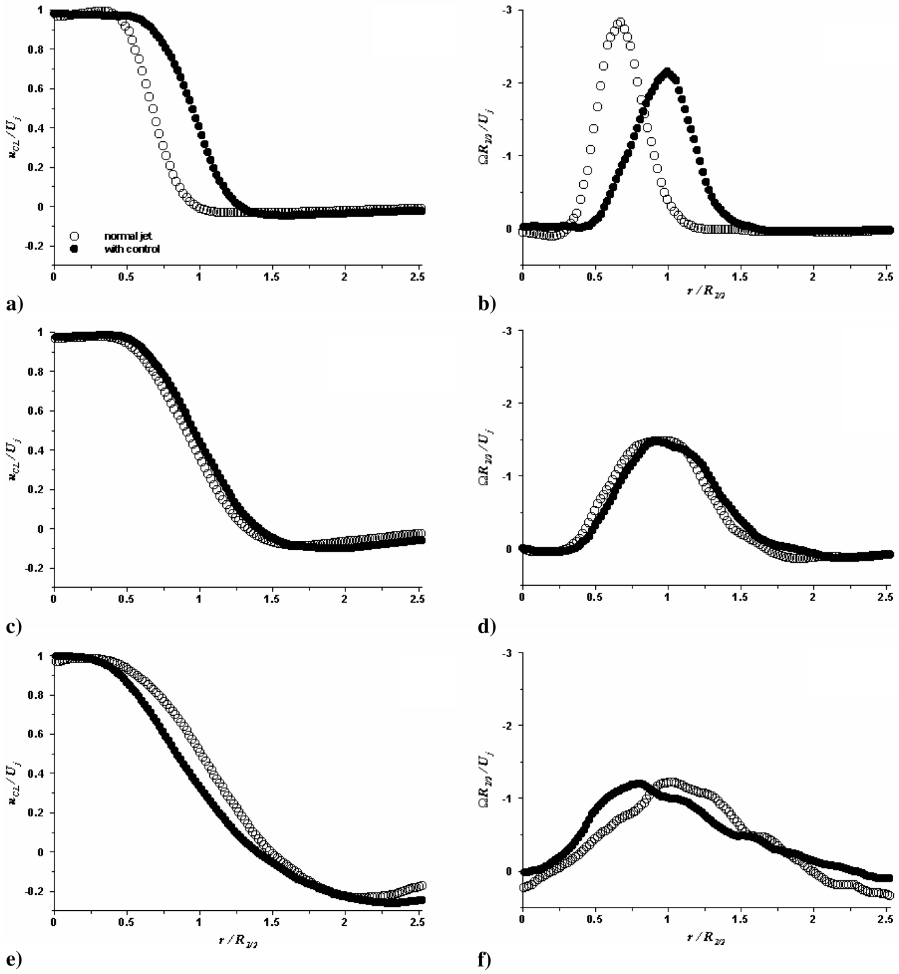

Fig. 19 Comparison of the mean axial velocity and vorticity profiles with and without control for $h/d_s = 4$; a) and b) $x/d_s = 1$, c) and d) $x/d_s = 2$, e) and f) $x/d_s = 3$.

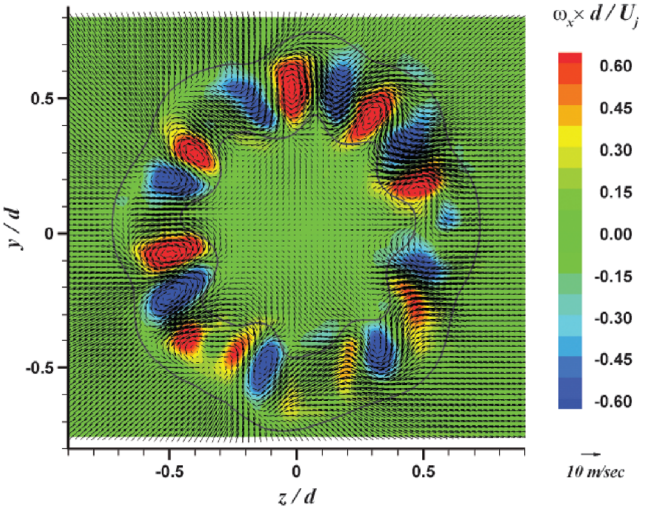

Fig. 20 Cross-plane streamwise vorticity distribution at $x/d = 1.75$; $M_j = 0.9$.

coincident with one of the jet centerlines ($y/d_s = 1.5$; $r = 0$). Because the mean flowfield is symmetric with respect to the central plane between the two jets, the profiles extend only to the location $y/d_s = 0$ (see Fig. 4). Velocity profiles in the vicinity of microjet injection produce a larger shear layer thickness with lower peak vorticity as shown in Figs. 19a and 19b. Based on jet stability considerations, Arakeri et al. [8] argued that velocity profiles with lower peak-normalized vorticity are more stable, resulting in large-scale spanwise structures with much reduced strength. At $x/d_s = 3$, the peak vorticity appears to be same with and without control, suggesting that the microjets' effect diminishes within few diameters (primary nozzle) of the nozzle exit. However, their effect on turbulence structure is felt further downstream, as will be shown in Sec. III.G.

The results discussed thus far indicate that the microjets are effective in reducing the overall unsteadiness of the jets and hence lead to a reduction in the noise. It is worthwhile to mention here briefly the physical mechanisms by which the microjets affect the aerodynamic characteristics of the twin impinging jets. It was recently demonstrated by Krothapalli et al. [1], and the references therein, that the adverse effects related to impinging jets are due to the strong feedback mechanism, and their reduction requires that this feedback loop be significantly weakened. There are several approaches for accomplishing this. For example, the feedback can be interrupted by intercepting the upstream and/or downstream propagating acoustic waves. This approach was adapted by Elavarasan et al. [22], who used a baffle/control plate just outside the nozzle exit to intercept the acoustic waves. In principle, one can also disrupt the feedback mechanism by changing the stability characteristics of the shear layer in the main jet(s).

The physical mechanisms behind the use of microjets for the control of impinging jets have been examined in some detail by Alvi et al. [2], Lou [9], and Lou et al. [23]. They argue that the efficacy of this technique lies in the fact that the microjets disrupt the feedback loop in more than one way, as follows. First, the feedback is weakened because the high-momentum microjets disrupt the coherence of the coupling between the acoustic waves and the main jet shear layer instabilities. Second, their detailed velocity-field measurements using PIV (Lou et al. [24] and Lou [9]) clearly show that the microjets produce well-organized pairs of streamwise, counterrotating vortices in the jet shear layer, quite similar to those shown in Fig. 20 [21]. The out-of-plane component of the vorticity field, obtained using stereoscopic PIV, in the cross plane of a $M_j = 0.9$ jet at $x/d = 1.75$ is shown. In this experiment [21], eight microjets exiting from 800-μm-diam tubes entered the primary jet at an angle of 60 deg to the jet axis at the circular nozzle exit with a diameter of 70 mm. The presence of streamwise vorticity, which is contained in two counterrotating vortices for each microjet, is vividly depicted in this figure with its normalized magnitude represented in color contours. Shear layer boundary is also shown in the figure by the contour lines representing the axial velocity values of $0.1U_j$ and $0.9U_j$. These streamwise structures weaken the primary, large-scale, azimuthal structures that are otherwise dominant in the jet shear layer. Because the impingement of these large-scale eddies on the ground plane are the principle sound source (Krothapalli et al. [1]), their attenuation weakens the feedback mechanism. Additionally, the counterrotating vortices generated by the microjets significantly increase the radial entrainment into the jet shear layer, very close to

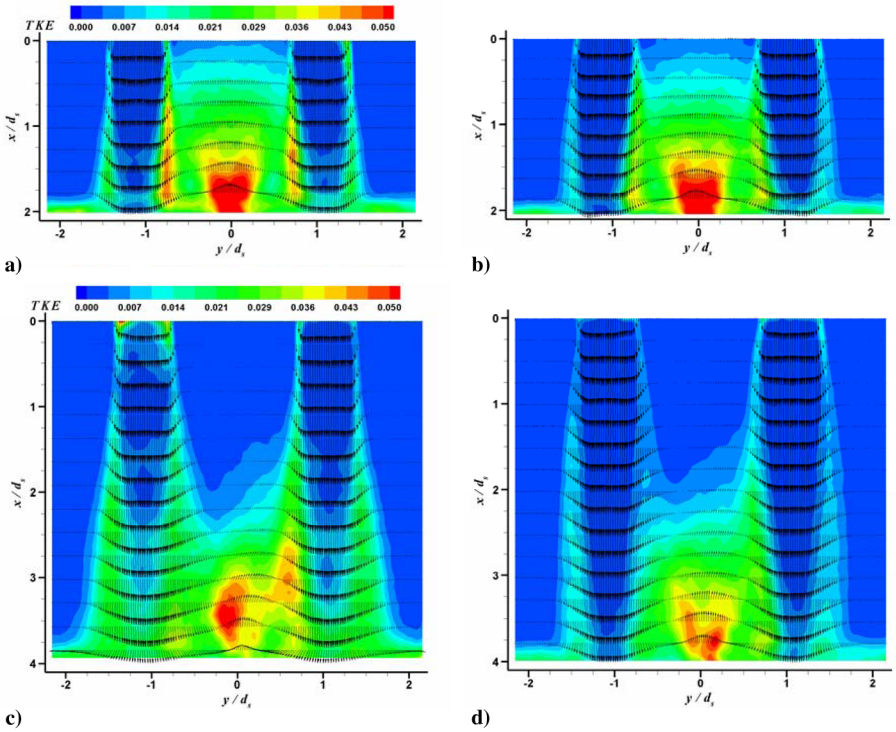

Fig. 21 Contour plots of TKE; a) normal jet at $h/d_s = 2$, b) with control at $h/d_s = 2$, c) normal jet at $h/d_s = 4$, d) with control at $h/d_s = 4$.

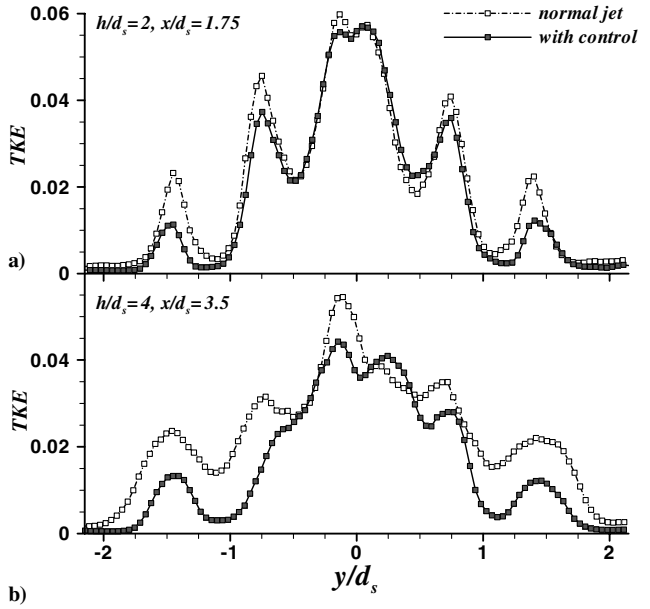

Fig. 22 Comparison of TKE profiles of normal jet and jet with control, a) $h/d_s = 2, x/d_s = 1.75$, b) $h/d_s = 4, x/d_s = 3.5$.

the nozzle exit. The result is a thicker shear layer near the nozzle exit, which is more stable and less receptive to the acoustic disturbances propagating upstream from the ground plane (Lou et al. [24] and Lou [9]). All of these effects are thought to play a collective role in efficiently disrupting the feedback mechanism using microjets.

G. Turbulence Characteristics

It is of interest to know the effectiveness of microjets in suppressing the turbulence within the shear layers, in the impingement region and the fountain flow. As a measure of the unsteadiness of the flow, the turbulence kinetic energy [$\mathrm{TKE} = (u'^2 + v'^2)/2U_j$] normalized by the fully expanded jet velocity is given in Fig. 21 for the jet conditions of Fig. 15. The magnitudes of the turbulence intensities for the controlled cases are substantially reduced in the shear layers and in the impinging region as compared to the normal jets. Especially in the outer shear layers the reduction is considerable. The decrease in the magnitudes of TKE in the jet column with microjet control is evident from the figure. The violent oscillations of the jet are totally eliminated, resulting in a more steady jet column as compared to the no-control case. In the fountain flow, however, for the two measured ground plane heights the fluctuations remain close to normal jet conditions with a subtle decrease.

The reduction in TKE is further examined by taking cross-plane profiles at downstream locations close to the ground plane (at $x/d_s = 1.75$ for the case $h/d_s = 2$ and at $x/d_s = 3.5$ for the case $h/d_s = 4$). The results of jet with control are compared to normal jet in Fig. 22. For ground plane height of $h/d_s = 2$ (shown in Fig. 22a) the maximum normalized TKE magnitudes are observed in the fountain flow region, reaching to the value of about 0.06 at the center. The other two peaks from the center correspond to the inner shear layer and outer shear layer of the twin jet columns. In the inner shear layer, the normalized values of TKE reach to about 0.04 and in the outer shear layer they reach to about 0.022.

When the microjet control is enabled, almost no change in TKE values can be observed in the fountain flow region of the flowfield. On the other hand, some reduction was clear in the inner shear layer

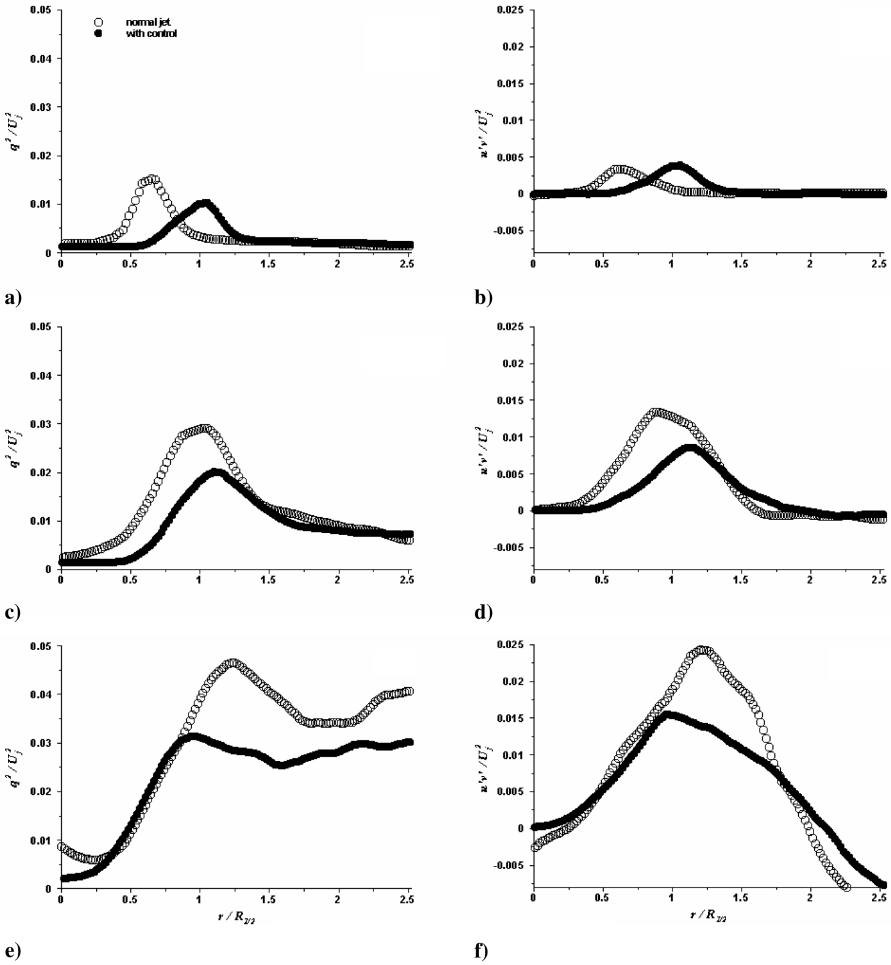

Fig. 23 Comparison of TKE and Reynolds stress profiles of normal jet and jet with control for $h/d_s = 4$; a) and b) $x/d_s = 1$, c) and d) $x/d_s = 2$, e) and f) $x/d_s = 3$.

(~20% at this x/d_s, and up to ~40% at upstream locations). The maximum reduction in TKE was in the outer shear layer region with reductions of about 50%. When the ground plane is moved to $h/d_s = 4$, in general, the fluctuation levels decreased as shown in Fig. 22b. The maximum TKE values were again in the fountain flow region with values of about 0.05. Although the peaks are not as distinct as the previous case, they can still be identified indicating the shear layer regions of the flowfield with peak values of around 0.03 and 0.025 for inner and outer shear layers, respectively. Similar to the previous ground plane height of $h/d_s = 2$, a subtle reduction was obtained in the fountain flow region of the jet with microjet control. But in general, the reductions in TKE are much broader, covering all the impinging region of the jets. In the shear layers, the normalized TKE values were decreased to 50% of the normal jet values, and within the jet column, fluctuations were almost eliminated (the jet column can be followed in the same contour color down to the ground plane in Fig. 21d). The flow visualization pictures show that the jet columns oscillate most vigorously at $h/d_s = 4$. Figure 23 shows the variation of the TKE (denoted by q^2) and the Reynolds stress at this location and across the cross planes ($x/d_s = 1$, 2, and 3) starting from the jet centerline ($r = 0$) and inwards. Both the quantities are normalized by the fully expanded jet velocity. Close to the nozzle exit, that is, at $x/d_s = 1$, the TKE and the Reynolds stress reach a normalized value of about 0.016 and 0.004, respectively. With the activation of microjets, there is a reduction of about 25% in the peak values of TKE, but there is no appreciable change in the Reynolds stress. It is also noticeable that the location at which the peak values occur is not the same for the normal jet and with microjet control. This is because of the thickening of the shear layer near the nozzle exit with the activation of microjets, which in turn causes the peak value to move outwards. At downstream locations, that is, at $x/d_s = 2$ and 3, the microjets cause a peak value reduction of about 38% in the TKE and about 42% in the Reynolds stress. This shows that the fluctuations in the impingement region are reduced to a considerable extent by the use of microjets.

Because these fluctuations play an important role on the sonic fatigue, it is essential that they are reduced and this study shows that microjets have been effective in decreasing these fluctuation levels. An examination of the turbulence production term, given by $u'v'(\mathrm{d}u/\mathrm{d}y)$ shows that with $\mathrm{d}u/\mathrm{d}y$ remaining the same, an increase in the magnitude of $u'v'$ increases the level of turbulence production in the jet. As seen from Fig. 23, the activation of microjets causes a reduction in the Reynolds stress values in the shear layers of the jet and hence indicates that the turbulence levels are also reduced. It is also known that a highly turbulent jet radiates more noise than a jet with lower levels of turbulence. A look at the OASPL values at $h/d_s = 4$ testifies to this fact by indicating a reduction in the noise levels with the activation of the microjets. Figure 23 further shows that the effect of the microjets is still seen further downstream (at $x/d_s = 3$), as indicated by a decrease in the peak values of TKE and Reynolds stresses.

It is interesting to note that even though the peak vorticity values (Fig. 19f) at $x/d_s = 3$ are about the same for both the normal jet and with control, the turbulence levels decrease with the introduction of microjets. The decrease in turbulence levels with microjet activation, as discussed earlier, is due to the absence of the large-scale eddies which are the source of unsteadiness in the normal jet. However, the presence of vorticity for the control case with magnitudes comparable to the normal jet case at $x/d_s = 3$, even though the large-scale eddies are absent, is a mere consequence of the increase in the velocity gradient as a result of increase in the main jet velocity (Fig. 18). In general, the microjets are effective in suppressing the turbulence levels in the twin impinging jets, the maximum reduction being the case at $h/d_s = 4$, where the jets oscillate most violently.

IV. Conclusions

The effect of a simple control technique on the acoustic and aerodynamic characteristics of ideally expanded twin impinging jet flowfield was investigated. As a control method, a set of microjets was used around the jet exit. Microphone and dynamic surface pressure measurements were used to observe the changes in the jet acoustics and sonic fatigue, and PIV and static surface pressure measurements were used to measure the aerodynamic characteristics of the jet in presence of the microjet control. The microjet control appears to change the shear layer characteristics and it eliminates the violent unsteady behavior of the shear layers. In addition, it prevents (or delays considerably) the formation of large-scale structures seen in impinging flows. Consequently a large reduction in the entrained flow is expected, which is believed to be the cause of suckdown forces. Similarly, because the large-scale structures play an important role in the generation of impinging tones, they were also eliminated with control. In addition, a small increase in the fountain velocity was observed. For certain ground plane heights, 25% lift loss recovery and 5 dB reduction in the near-field OASPL was observed.

Acknowledgments

We would like to thank NASA Ames Research Center for supporting this work. We would also like to thank Jim Ross and Doug Wardwell for their continued interest in this problem. The suggestions given by F. Alvi are greatly appreciated.

References

[1] Krothapalli, A., Rajakuperan, E., Alvi, F., and Lourenco, L., "Flow Field and Noise Characteristics of a Supersonic Impinging Jet," *Journal of Fluid Mechanics*, Vol. 392, 1999, pp. 155–181.

[2] Alvi, F. S., Elavarasan, R., Shih, C., Garg, G., and Krothapalli, A., "Control of Supersonic Impinging Jet Flows Using Microjets," *AIAA Journal*, Vol. 41, No. 7, 2003, pp. 1347–1355.

[3] Kuhn, R. E., "V/STOL and STOL ground effects and testing techniques," *Proceedings of the 1985 NASA Ames Research Center's Ground-Effects Workshop*, edited by Kerry Mitchell, CP 2462, NASA, 1987.

[4] Lummus, J. R., and Smith, E. W., "Flow Field Characteristics and the Effect of Jet-Exhaust Simulation for V/STOL Vehicles Near the Ground," *Proceedings of the NADC V/STOL Aircraft Aerodynamics Symposium*, Naval Post Graduate School, Monterey, CA, 1979, pp. 293–313.

[5] Saripalli, K. R., "Visualisation of Multijet Impingement Flow," *AIAA Journal*, Vol. 21, No. 4, 1983, pp. 483–484.

[6] Krothapalli, A., "Twin Supersonic Impinging Rectangular Jets," *Proceedings of the 1985 NASA Ames Research Center's Ground-Effects Workshop*, edited by K. Mitchell, CP 2462, NASA, 1987.

[7] Elavarasan, R., Venkatakrishnan, L., Krothapalli, A., and Lourenco, L., "Supersonic Twin Impinging Jets," AIAA Paper 2000-0812, 2000.

[8] Arakeri, V. H., Krothapalli, A., Siddavaram, V., Alkislar, M., and Lourenco, L., "On the Use of Microjets to Suppress Turbulence in a Mach 0.9 Axisymmetric Jet," *Journal of Fluid Mechanics*, Vol. 490, 2003, pp. 75–98.

[9] Lou, H., "Control of Supersonic Impinging Jet Using Microjets," Ph.D. Dissertation, Florida State Univ., Tallahassee, FL, 2005.

[10] Wardwell, D. A., Hange, C., Kuhn, R. E., and Stewart, V. R., "Jet-Induced Ground Effects on Parametric Flat-Plate Model in Hover," NASA Technical Memorandum 104001, 1993.

[11] Lourenco, L., and Krothapalli, A., "True Resolution PIV: A Mesh-Free Second-Order Accurate Algorithm," *Proceedings of the 10th International Symposium on Applications of Laser Techniques in Fluid Mechanics*, Lisbon, 2000 (Paper 13.5).

[12] Alkislar, M. B., Krothapalli, A., and Lourenco, L. M., "Structure of a Screeching Rectangular Jet: A Stereoscopic PIV Study," *Journal of Fluid Mechanics*, Vol. 489, 2003, pp. 121–154.

[13] Tam, C. K. W., "Supersonic Jet Noise," *Annual Review of Fluid Mechanics*, Vol. 27, 1995, pp. 17–43.

[14] Alkislar, M. B., Krothapalli, A., Choutapalli, I., and Lourenco, L. M., "Structure of Supersonic Twin Jets," *AIAA Journal*, Vol. 43, No. 11, 2005, pp. 2309–2318.

[15] Seiner, J. M., Manning, J. C., and Ponton, M. K., "Dynamic Pressure Loads Associated with Twin Supersonic Plume Resonance," *AIAA Journal*, Vol. 26, No. 8, 1988, pp. 954–960.

[16] Green, M. R., and Crighton, D. G., "Instability Properties of Interacting Jets," *Journal of Fluid Mechanics*, Vol. 350, 1997, pp. 331–349.

[17] Raman, G., and Taghavi, R., "Coupling of Twin Rectangular Supersonic Jets," *Journal of Fluid Mechanics*, Vol. 354, 1998, pp. 123–146.

[18] Alvi, F. S., Krothapalli, A., Washington, D., and King, C. J., "Aeroacoustic Properties of a Supersonic Diamond-Shaped Jet," *AIAA Journal*, Vol. 34, No. 8, 1996, pp. 1562–1569.
[19] Powell, A., "On Edge Tones and Associated Phenomena," *Acustica* Vol. 3, 1953, pp. 233–243.
[20] Wilkinson, J. E., Lu, H. Y., and Seiner, J. M., "The Noise Shielding Effects of Multiple Jets," CEAS/AIAA Paper CEAS/AIAA-95-068, 1995.
[21] Siddavaram, V., "Flow Characterization of a Mach 0.9 Axisymmetric Jet Using Particle Image Velocimetry," M.S. Thesis, Dept. of Mechanical Engineering, Florida State Univ., Tallahassee, FL, 2002.
[22] Elavarasan, R., Krothapalli, A., Venkatakrishnan, L., and Lourenco, L., "Suppression of Self-Sustained Oscillations in a Supersonic Impinging Jet," *AIAA Journal*, Vol. 39, No. 12, 2000, pp. 2366–2373.
[23] Lou, H., Alvi, F. S., and Shih, C., "Active and Passive Control of Supersonic Impinging Jets," *AIAA Journal*, Vol. 44, No. 1, 2006, pp. 58–66.
[24] Lou, H., Shih, C., and Alvi, F., "A PIV Study of Supersonic Impinging Jet," AIAA Paper 2003-3263, 2003.

A. Karagozian
Associate Editor